



The Effects of Plasma Lensing on the Inferred Dispersion Measures of Fast Radiobursts

Xinzhong Er¹ , Yuan-Pei Yang¹ , and Adam Rogers² ¹ South-Western Institute for Astronomy Research, Yunnan University, Kunming, Yunnan, People's Republic of China; xer@ynu.edu.cn² Department of Physics and Astronomy, University of Manitoba, Winnipeg, MB, R3T 2N2, Canada

Received 2019 September 5; revised 2019 December 29; accepted 2019 December 31; published 2020 February 4

Abstract

Radio signals are delayed when propagating through plasma. This type of delay is frequency dependent and is usually used for estimating the projected number density of electrons along the line of sight, called the dispersion measure (DM). The dense and clumpy distribution of plasma can cause refractive deflections of radio signals, analogous to lensing effects. Similar to gravitational lensing, there are two contributions to the time delay effect in plasma lensing: a geometric delay, due to increased path length of the signal, and a dispersive delay due to the change of speed of light in a plasma medium. We show the delay time for two models of the plasma distribution, and point out that the estimated DM can be biased. Since the contribution of the geometric effect can be comparable to that of the dispersive delay, the bias in the measured DM can be dramatically large if plasma lensing effects are not taken into account when signals propagate through a high-density gradient clump of plasma.

Unified Astronomy Thesaurus concepts: [Interstellar medium \(847\)](#); [Strong gravitational lensing \(1643\)](#); [Radio transient sources \(2008\)](#)

1. Introduction

Fast radiobursts (FRBs) are a new kind of radio transient with millisecond duration. These mysterious events are characterized by an excess dispersion measure (DM) with respect to the Galactic contribution as well as high brightness. Evidence is emerging that FRBs are distributed isotropically on the sky (e.g., Thornton et al. 2013; Shannon et al. 2018; Cordes & Chatterjee 2019), however the physical origin of these bursts is still unknown. At the time of writing, the total number of the published FRBs is around 100 (see FRB Catalog³ of Petroff et al. 2016). Several of these bursts show repeating behaviors, including FRB 121102 (Spitler et al. 2016; Chatterjee et al. 2017) and FRB 180814 (CHIME/FRB Collaboration et al. 2019), and eight FRBs recently discovered by the Canadian Hydrogen Intensity Mapping Experiment (CHIME; Casertini et al. 2019; The CHIME/FRB Collaboration et al. 2019). Thanks to interferometric localizations, FRB 121102, FRB 180924, FRB 181112, and FRB 190523 have been localized to sufficient accuracy to identify their host galaxies (Chatterjee et al. 2017; Bannister et al. 2019; Prochaska et al. 2019; Ravi et al. 2019). The first repeating burst, FRB 121102, has been found to be located in a star-forming dwarf galaxy at $z = 0.19273$ and associated with a persistent radio source (Chatterjee et al. 2017; Marcote et al. 2017; Tendulkar et al. 2017). FRB 180924 is localized to a position 4 kpc from the center of a luminous galaxy at redshift $z = 0.3214$ (Bannister et al. 2019). FRB 190523 is found to be associated with a massive galaxy with low specific star-formation rate at a redshift of $z = 0.66$ (Ravi et al. 2019). Since DM and redshift have been measured for these FRBs, they can be used as an intergalactic and cosmological probe (e.g., Deng & Zhang 2014; Yang & Zhang 2016; Yang et al. 2017; Zhang 2018; Li et al. 2019b).

As with any radio transients at cosmological distance, FRBs are dispersed when they propagate in ionized gas, i.e., free electrons. Generally, the lower the frequency of a signal, the

longer the delay time, which has been found in all FRB observations. To describe this behavior, let us define Δt as the delay time⁴ of a burst at frequency ν . The delay time–frequency relation of FRBs is nearly consistent with the classical dispersion of an electromagnetic wave in cold plasma (Lorimer et al. 2007), $\Delta t \propto \text{DM}\nu^{-2}$, where DM directly reflects the free electron column density along the line of sight, e.g., $\text{DM} \equiv \int n_e dl$. A slight discrepancy from the quadratic time delay relationship has been found through observations (e.g., Thornton et al. 2013; Katz 2016), suggesting the plasma may also be emitting (e.g., Cordes & Chatterjee 2019). For FRBs, one of the most important features is the excess DM with respect to the Milky Way's contribution, suggesting that the bursts have a cosmological origin (Thornton et al. 2013).

Generally, since FRBs seem to be isotropically distributed over the sky, we expect refractive lensing to occur due to a chance alignment of an FRB source with a foreground lens object. The lens may be a small plasma inhomogeneity within the host galaxy of the FRB (Cordes et al. 2017), an intervening astrophysical object (e.g., galaxy or cluster) halo may act as a strong gravitational lens (Li & Li 2014; Dai & Lu 2017; Li et al. 2018; Wang & Wang 2018), or an isolated and extragalactic compact object may act as a gravitational microlens (Zheng et al. 2014; Muñoz et al. 2016). In particular, Prochaska et al. (2019) recently found that FRB 181112 passed through a foreground galaxy halo, and they proved that the burst observation characteristics can be used to constrain the plasma properties (e.g., magnetic field and turbulence). In addition, the probability of a radio signal propagating through a clump of plasma within the Milky Way is also high (Cordes & Lazio 2002). We therefore consider three possible locations for plasma lenses: within the Milky Way, an intervening galaxy or galaxy cluster, and within the host galaxy. In the case of an intervening galaxy, we assume the galaxy is not sufficiently

⁴ In gravitational lensing, the time delay sometimes refers to the difference in the arrival times between multiple lensed images. In this work, the time delay represents the delay in excess of the unlensed case. This is equivalent to measuring time delay with respect to the arrival time of the signal in the high frequency limit.

³ <http://frbcatalog.org/>

aligned with the line of sight to substantially contribute any gravitational lensing effect, but that a plasma inhomogeneity within the galaxy is sufficiently positioned to act as a lens to the distant source.

Plasma lensing plays an important role in the ‘‘Extreme Scattering Events’’ (ESEs) that are seen in the light curves of some active galactic nuclei and pulsars. Plasma lensing is the phenomenon of radiation traveling along deflected paths due to the variable electron density across the plane of the sky (e.g., Rossi & Twersky 1957; Cognard et al. 1993). These ESEs are consistent with plasma lensing from \sim astronomical unit (au) structures in the Milky Way (e.g., Fiedler et al. 1987; Pen & King 2012; Pushkarev et al. 2013; Pen & Levin 2014; Coles et al. 2015). Several models of plasma lenses have been proposed from analytical distributions or by fitting the observations (e.g., Romani et al. 1987; Rickett 1990; Clegg et al. 1998; Bannister et al. 2016; Liu et al. 2016; Tuntsov et al. 2016; Er & Rogers 2018), and even include magnetic fields (e.g., Li et al. 2019a). It has been also suggested that pulsar scintillation is caused by scattering due to plasma structures (e.g., Stinebring et al. 2001; Cordes et al. 2006, 2016; Coles et al. 2010; Kerr et al. 2018; Lam et al. 2018; Simard & Pen 2018; Simard et al. 2018; Gwinn 2019). Recently, Cordes et al. (2017) proposed that the amplitude of an FRB can be strongly modulated by plasma lenses in the host galaxy. The complex properties of plasma lenses might account for the observations of repeating FRBs. For example, strong focusing by plasma lenses can produce large intensity variations with factors of 10–100, which might account for the intermittency seen from FRB 121102 (Cordes et al. 2017; Hessels et al. 2018). If a plasma lens acts on an FRB that is observed as a repeater, the properties of the plasma lens, including lens size, density, and transverse velocity, can be constrained by the observation of the DM variation of the repeating FRBs (Yang & Zhang 2017).

Similar to gravitational lensing (Schneider et al. 1992), plasma lensing also causes time delays. In contrast to gravitational lensing, plasma lensing leads to different observable phenomena. For instance, suppose the deflection caused by plasma lensing of a background source is small. Then the image separations between the multiple images (if multiple imaging occurs at all), are extremely difficult to resolve. In this case, the time delay between images in a lensing system are unlikely to be directly measured due to their tiny angular separation. However, in plasma lensing, the time delay is frequency dependent, offering an entirely unique avenue to study the structure of the lens and the source. Moreover, plasma lenses are very versatile in terms of their magnification properties. Generally plasma acts like a diverging lens responsible for demagnification of background sources. However, the particular geometry of a lens, source, and observer, can also cause substantial magnification to occur (e.g., Dong et al. 2018; Er & Rogers 2018; Kerr et al. 2018). Plasma lenses that are under-dense compared to the surrounding interstellar medium (ISM) behave like converging lenses and magnify background sources (e.g., Pen & King 2012).

The frequency dependent delay caused by plasma lenses shows behavior that is distinct from the classical dispersion relation, since the change of path length causes an extra delay in the propagation of the signal, i.e., a geometric delay. As we will see in the next sections, the geometric delay is proportional to the square of the deflection angle, and thus has a dependence

on wavelength to the fourth power. When the gradient of the plasma density is large, the geometric term can dominate the total delay time. For instance, the two-dimensional dynamic power spectra of some pulsars show organized parabolic structures, which suggests significant geometric contributions to the time delay (Stinebring et al. 2001; Stinebring 2007). Moreover, it has been noted that the DM variations with frequency can be used to study sub-structures in the ionized ISM (e.g., Cordes et al. 2016; Donner et al. 2019; Lam et al. 2019, and references therein). Therefore, if an FRB passes through such an ionized sub-structure in the ISM, the frequency-dependent delay time of plasma lensing would affect the observed apparent dispersion relation of the FRB. Plasma lensing can also induce other frequency-dependent effects, such as displacement, magnification (scintillation), and distortion in the multiple images of a background source.

In this work, we focus on the delay time of FRBs induced by various plasma lens models, including exponential and power-law (PL) models. In addition, we consider the possibility that the lens may reside in the Milky Way, in the FRB host galaxy, or in an intervening galaxy. In Section 2, we briefly introduce the theory and formulae of plasma lensing. Two models of lensing are shown in Sections 3 and 4. We discuss the possible bias plasma lensing introduces to the estimation of dispersion relation and finally summarize our results. In this paper we adopt the standard Λ CDM cosmology with parameters based on the results from the *Planck* data (Planck Collaboration et al. 2016): $\Omega_\Lambda = 0.6791$, $\Omega_m = 0.3209$, and Hubble constant $H_0 = 100h$ km s $^{-1}$ Mpc $^{-1}$ and $h = 0.6686$.

2. Basic Formulae of Plasma Lensing

The description of gravitational lensing used in this work follows from Schneider et al. (1992) and Narayan & Bartelmann (1996). We make the usual thin lens approximation, which means that we assume weak deflection, and the scattering occurs only on the lens plane. We consider a source at angular position β with respect to the line of sight, and the corresponding image is formed at the angular position θ . The angular diameter distance from the observer to source, deflecting lens, and the difference between are given by D_s , D_d , and D_{ds} , respectively. The lens equation can be written as

$$\beta = \theta - \alpha = \theta - \nabla_\theta \psi(\theta), \quad (1)$$

where α is the deflection angle, ψ is the effective lens potential, and ∇_θ is the gradient on the image plane. Lens models based on both analytical and numerical approaches have also been explored (e.g., Tuntsov et al. 2016; Cordes et al. 2017; Er & Rogers 2018). When an electromagnetic wave propagates through a plasma lens, it will be delayed due to two separate effects. First, a signal is delayed due to the increasing path length of propagating along a trajectory that has been deflected by a plasma lens. This is the geometric component of the time delay. Second, an electromagnetic wave propagating through plasma is also delayed due to dispersion, the frequency-dependent change of velocity of the signal. This is the effective ‘‘potential’’ delay, analogous to the Shapiro delay in gravitational lensing. Unlike gravitational lensing, both terms of the delay due to plasma are frequency dependent. In particular the geometric effect, which is affected by the distribution of the plasma, shows stronger dependence on the frequency.

We consider the geometric effect due to the light ray being deflected by a clump of plasma.⁵ Then the delay time contributed by the geometric effect is given by (e.g., Blandford & Narayan 1986; Cordes et al. 2017).

$$T_{\text{ge}} \simeq \frac{(1+z_d) D_d D_s (\beta - \theta)^2}{c D_{ds} 2}. \quad (2)$$

Next, we consider the contribution from electromagnetic wave dispersion in plasma. The refractive index of cold plasma for a radio wave with angular frequency $\omega = 2\pi\nu$ is given by

$$n_{\text{pl}}^2 \equiv 1 - \frac{\omega_p^2}{\omega^2}, \quad (3)$$

where

$$\omega_p \equiv \sqrt{\frac{4\pi e^2 n_e}{m_e}} \quad (4)$$

is the plasma frequency, e is the electron charge, m_e is the mass of the electron, and n_e is the number density of electrons in the plasma. Thus, the delay time due to wave dispersion is given by

$$T_{\text{pl}} = \int \frac{1}{c} \left(\frac{1}{n_{\text{pl}}} - 1 \right) dl. \quad (5)$$

In general, the plasma frequency is much smaller than the observational frequency $\omega_p \ll \omega$. The propagation delay time can be approximated as

$$T_{\text{pl}} \simeq \int_0^r \frac{\omega_p^2}{2c\omega^2} dl = \frac{2\pi cr_e}{\omega^2} \text{DM}(\theta), \quad (6)$$

where r_e is the classical electron radius, and $\text{DM}(\theta)$ is known as the dispersion measure:

$$\text{DM}(\theta) \equiv \int_0^{D_s} n_e(\theta, l) dl. \quad (7)$$

We work with the Born approximation for weak deflection angles, relevant for both gravitational and plasma lensing in the geometric optics limit. Thus, the deflection angles are small and the integrals can be done along unperturbed rays. For great distances, the DM is approximated by the projected electron density along the line of sight, $\text{DM}(\theta) \approx N_e(\theta)$. In reality, the dispersive delay is caused by frequency-dependent refraction of the wave through the inhomogeneous plasma. This causes radio signals at different frequencies to have different paths and thus experience different projected density of electrons (DM); while N_e is the projected density along a straight line of sight. Only when the electron distribution is uniform, i.e., no deflection of radio signals occurs, are the two quantities exactly equal. Both notations will be used interchangeably in this work.

Combining Equations (2) and (6), the total time delay can be written as the sum of two terms

$$T(\theta, \beta) = \frac{(1+z_d) D_d D_s (\beta - \theta)^2}{c D_{ds} 2} + \frac{2\pi cr_e}{\omega^2} N_e(\theta). \quad (8)$$

⁵ In this work, we only consider the geometric optics limit. For the extreme low-frequency signal, wave effects need to be taken into account.

We define the ‘‘effective plasma lens potential’’ by

$$\psi(\theta) \equiv \frac{1}{(1+z_d)} \frac{D_d D_s}{D_d D_s} \frac{\lambda^2}{2\pi} r_e N_e(\theta). \quad (9)$$

In a similar fashion to gravitational lensing. We will use the geometric term and the dispersive term for the two contributions to the time delay in this work. The geometric delay is proportional to $\alpha^2 \propto \lambda^4$ and is more sensitive to the wavelength than the dispersive delay, i.e., $\psi \propto \lambda^2$.

For FRBs, the observed contribution to the DM from the lens is summarized in (e.g., Yang & Zhang 2016)

$$\text{DM}_{\text{obs}} = \text{DM}_{\text{MW}} + \text{DM}_{\text{IGM}} + \text{DM}_{\text{HG}}, \quad (10)$$

where DM_{MW} , DM_{IGM} , and DM_{HG} denote the contributions from the Milky Way, intervening galaxy, and the host galaxy of the FRB, respectively. The plasma lensing effects from individual contributions can vary significantly due to the distance, especially the geometric delay. We will discuss such effects in the following sections for different models of electron density and lens distances. In this work, we assume the source is at the redshift of one repeated FRB (Spitler et al. 2016), which is $z_s = 0.19273$ (~ 690.053 Mpc), and compare the cases of the plasma lens at different distances: Milky Way ($z = 5 \times 10^{-7} \sim 2.24$ kpc), intervening galaxy ($z = 0.05 \sim 210$ Mpc), and FRB host galaxy ($z = 0.192729 \sim 690.05$ Mpc). Due to the difficulty of both theory and observation of the ISM on the spatial scales necessary for ESEs, there are no analytical or empirical expressions for the detailed density structure of the plasma. In this work we adopt two analytical forms for the spherically symmetric electron distribution within a plasma lens, which are widely used in the literature. The exponential models are a family of lenses that include the most well-known model, the Gaussian lens (e.g., Clegg et al. 1998; Bannister et al. 2016; Cordes et al. 2017), as well as the family of PL models (Er & Rogers 2018). These lens families are useful because they can be used as building blocks to construct more complicated density distributions.

3. Exponential Model

In this work, we restrict our study to axisymmetric models for the electron distribution in order to simplify the mathematics and provide clear, easy to interpret results. Additionally, we only adopt a single lens along the line of sight. Exponential lenses are a natural group of models to consider. The Gaussian lens introduced by Clegg et al. (1998) to describe observations of the extragalactic sources 0954+654 and 1741–038, is a special case of the exponential model ($h = 2$). We follow the description of exponential models in Er & Rogers (2018) and the Gaussian lens in Clegg et al. (1998). We adopt a form for the electron column density in the lens plane,

$$N_e(\theta) = N_0 \exp\left(-\frac{\theta^h}{h\sigma^h}\right) \quad (\theta > 0), \quad (11)$$

with N_0 the maximum electron column density within the lens, and σ the width of the lens for $h > 0$ (Vedantham et al. 2017).

The projected electron density gives the potential

$$\psi(\theta) = \theta_0^2 \exp\left(-\frac{\theta^h}{h\sigma^h}\right), \quad (12)$$

and deflection angle

$$\alpha(\theta) = -\theta_0^2 \frac{\theta^{(h-1)}}{\sigma^h} \exp\left(-\frac{\theta^h}{h\sigma^h}\right), \quad (13)$$

with the characteristic angular scale

$$\begin{aligned} \theta_0 &= \lambda \left(\frac{D_{ds}}{D_s D_d} \frac{1}{2\pi(1+z_d)} r_e N_0 \right)^{\frac{1}{2}} \\ &= \frac{c}{\nu} \left(\frac{D_{ds}}{D_s D_d} \frac{1}{2\pi(1+z_d)} r_e \text{DM}(0) \right)^{\frac{1}{2}}, \end{aligned} \quad (14)$$

where λ is the observing wavelength and ν is the frequency. The wavelength of a photon λ can vary in the gravitational field via the gravitational redshift effect, which introduces an additional complication to the deflection angle. Since we only focus on lensing from plasma, the gravitational deflection generated by the ISM will be neglected. The ratio of geometric to dispersive delay η can be given analytically

$$\eta = \frac{1}{2} \frac{\alpha^2}{\psi} = \theta_0^2 \frac{\theta^{2h-2}}{2\sigma^{2h}} \exp\left(-\frac{\theta^h}{h\sigma^h}\right). \quad (15)$$

In the case of $h \neq 1$, the ratio reaches a maximum at $\theta = (2h - 2)^{1/h} \sigma$. The maximum ratio is

$$\begin{aligned} \eta &= \frac{(2h - 2)^{\frac{2h-2}{h}} \theta_0^2}{2\sigma^2} \exp\left(-\frac{2h - 2}{h}\right) \\ &\propto \frac{\lambda^2}{(1+z_d)} \frac{D_{ds}}{D_d D_s} \frac{\text{DM}(0)}{\sigma^2}. \end{aligned} \quad (16)$$

Besides the wavelength, distance, DM, and h , the ratio is inversely proportional to the width of the lens σ^2 . Since the smaller σ , the larger the density gradient, the geometric effect becomes stronger.

The strength of the lens can be characterized by θ_0 . The relationship between θ_0 and σ determines the number of caustic curves in the source plane that separate areas of different image multiplicity (Rogers & Er 2019). We note that θ_0 depends on the frequency of observation, the number density of electrons as well as the distance of the lens and the source. In order to clearly see these dependencies, we present θ_0 in Figure 1. In this plot, we give the values of θ_0 for the plasma lens in an intervening galaxy at $z = 0.05$. The inverse dependence of θ_0 on the redshift can easily be seen from Equation (14). Suppose that we choose a large plasma clump to act as our lens, with $\sigma = 10^5$ au, and a conservative DM range: 20–200 pc cm⁻³ compared with the observations of FRBs (see the FRB catalog).⁶ In this case, the average density enhancement within the lens is a few tens of electrons due to the volume of such a large lens. A smaller σ means the clump is denser, with higher electron density, but the geometric term in the time delay is stronger (Equation (16)). For lenses at different redshift, θ_0 will

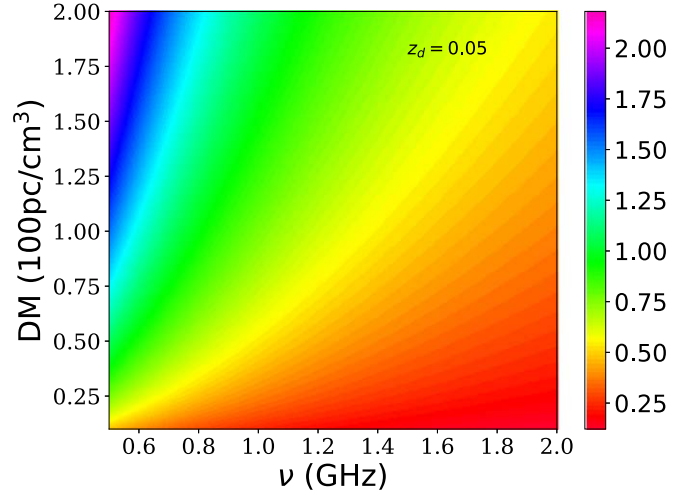


Figure 1. θ_0 (in unit of milli-arcsec) dependence on frequency and DM for the plasma lens of exponential model ($h = 2$) with lens redshifts $z = 0.05$ (intervening galaxy).

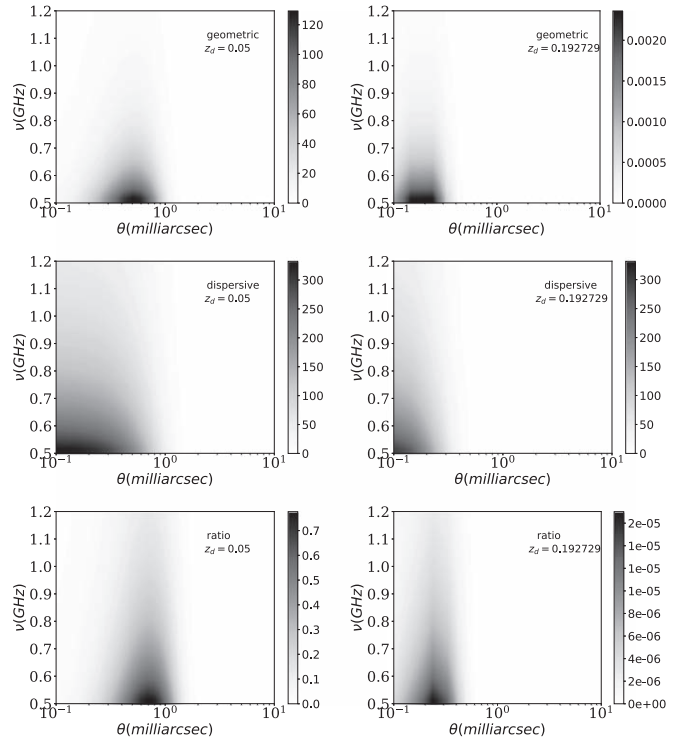


Figure 2. Delay time due to the geometric effect (top), dispersive effect (middle), and the ratio between the two (bottom) as a function of the image position θ and observational frequency. The time delay is shown in gray scale with units of milliseconds. In all the panels, we adopt the same exponential plasma lens parameters: $N_0 = 20$ pc cm⁻³, $\sigma = 10^5$ au, $h = 2$, but at the different lens redshifts. On the left (right) column, the lens redshift is 0.05 (0.192729).

show similar dependence on the observational frequency and DM, but will have a numerically distinct value with a generally different order of magnitude. We show the time delay caused by a plasma lens in Figure 2. For lenses at different redshift, the time delay caused by the dispersive term has the same order of magnitude, as it is approximately proportional to the projected electron density, although the angular size of the lensing region, the lens cross section, differs significantly due to the redshift of the lens. On the other hand, the geometric delay

⁶ In this work, we consider all of the DM to be contributed by one plasma structure along the line of sight. In reality, all the plasma clumps along the line of sight need to be taken into account, which requires a study using multiple lens planes. We will leave this more general scenario for future work.

Table 1

The Approximate Dependence of Two Time Delay Terms on the Parameters of the Exponential Lens Model

Parameter	Geometric Term	Dispersive Term
...	$\propto \alpha^2$	$\propto \psi$
N_0	$\propto N_0^2$	$\propto N_0$
λ	$\propto \lambda^4$	$\propto \lambda^2$
σ	$\propto 1/\sigma^{2h}$	$\propto \exp(-1/(h\sigma^h))$

shows a dramatic difference. When the lens is located at the middle point between us and the source, the geometric effect can contribute a time delay of similar order to that of dispersive delay, but has different dependence on the image position(θ), i.e., the delay time caused by the dispersive term reaches the maximum at the peak of the projected density, and the delay time caused by the geometric term reaches the maximum when the gradient of the density peaks. The ratio of geometric to the dispersive delay is shown in the bottom panel, demonstrating under which conditions it is safe to neglect the geometric delay. When the lens is in the Milky Way (the host galaxy), the geometric term becomes much smaller (see the right panel in Figure 2). If the density gradient is large, the geometric delay can contribute a significant part as well.

The geometric term strongly depends on the model parameters of the lens, in our case the width σ and charge density N_0 . From Table 1, the lens parameters affect the two delay terms in different ways. Another interesting point is that the geometric delay is proportional to λ^4 , which is independent of the lens properties. In Figure 3, the ratio between two delays for lenses at $z = 0.05$ are shown. As expected, when the gradient becomes significantly large, the geometric term can dominate over the dispersive term. A plasma lens in the Milky Way is slightly different from the other two cases. First, the probability that the FRB signal propagates through a clump of plasma in the Milky Way is high. Second, the small spatial variations of the plasma clump can cause substantial lensing effects. It has been suggested that the scale of the ISM clumps varies from 0.1 au to a few hundred au (Stanimirović & Zweibel 2018). We thus choose a small scale lens with $\sigma = 50$ au, and show two separate plots for lenses within our Galaxy in Figure 4. The units for the horizontal axis are different from previous figures, since the cross section of these lenses are large. Due to the small scale variations in the plasma, even for a small $DM_0 = 1$, the geometric delay can essentially equal the dispersive delay.

4. Power-law Model

The PL model serves as a useful example for the density profiles in gravitational lensing (Keeton 2001) and plasma lensing (Er & Rogers 2018). This is not only due to its well studied analytical behavior, but also because combinations of PL profiles can be built to mimic other more complex profiles and give rise to interesting optical properties. The three-dimensional electron density is given by

$$n_e(r) = n_0 \frac{R_0^h}{r^h}, \quad (17)$$

where n_0 is the density at radius $r = R_0$. The corresponding DM_0 can also be given for the projected density at $r = R_0$. However, usually R_0/D_d is much larger than θ_0 , so DM_0 does

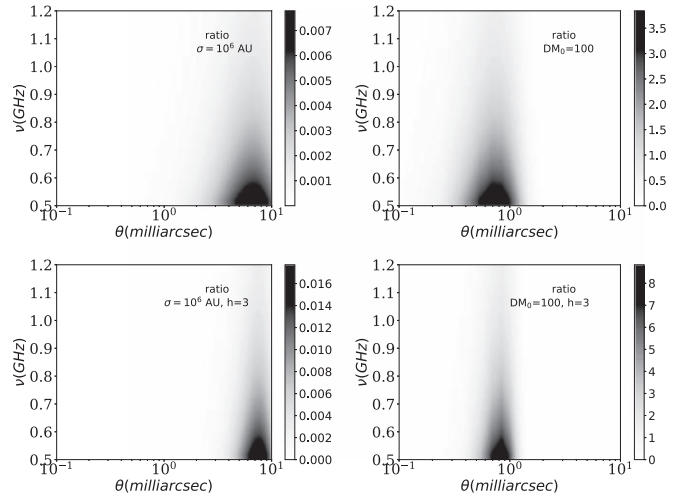


Figure 3. Ratio of geometric to dispersive delay for a lens at $z_d = 0.05$. The same lens parameters are adopted as Figure 2 except that given in the corner of each panel.

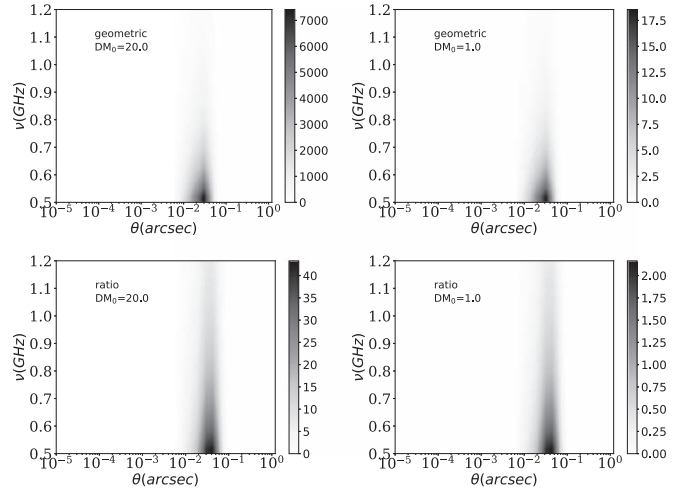


Figure 4. Same as Figure 2, but for plasma lenses at the Milky Way. Different lens parameters ($\sigma = 50$ au and DM is given in each panel) are adopted in this figure.

not describe the density where we are interested. In order to avoid the singularity at the center, we include a finite core with angular core radius θ_C . The plasma lens potential of the softened power-law (SPL) can thus be written as

$$\psi(\theta) = \frac{\theta_0^{h+1}}{(h-1)(\theta^2 + \theta_C^2)^{\frac{h-1}{2}}}, \quad h \neq 1, \quad (18)$$

with the characteristic angular scale (Bisnovatyi-Kogan & Tsupko 2009, 2015)

$$\theta_0 = \left(\lambda^2 \frac{D_{ds}}{(1+z_d)D_s D_d^h} \frac{r_e n_0 R_0^h}{\sqrt{\pi}} \frac{\Gamma\left(\frac{h}{2} + \frac{1}{2}\right)}{\Gamma\left(\frac{h}{2}\right)} \right)^{\frac{1}{h+1}}. \quad (19)$$

The SPL lens with $h = 1$ and the point-like plasma lens model have different forms of the potential. The SPL potential gives

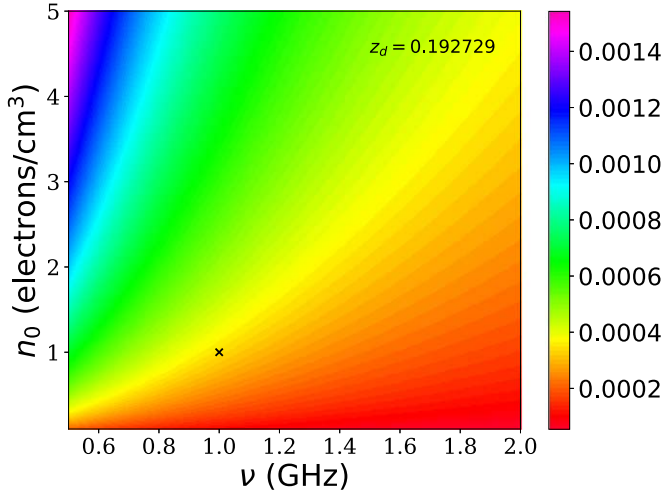


Figure 5. θ_0 for the PL model with $h = 1$, $R_0 = 10^6$ au. The black cross marks the value given in Table 2. In this lens configuration, $n_0 = 1 \text{ cm}^{-3}$ corresponds to column density $\text{DM}_0 \sim 5 \text{ pc cm}^{-3}$.

Table 2

θ_0 (milli-arcsec) for PL Model of Lens with $n_0 = 1 \text{ cm}^{-3}$, $\nu = 1 \text{ GHz}$, $R_0 = 10^6$ au

	$z = 5e - 7$	$z = 0.05$	$z = 0.192729$
$h = 1$	86.5	0.241	$3.46e-4$
$h = 2$	1741	0.758	$6.49e-3$
$h = 3$	7412	1.28	0.0267

the deflection angle

$$\alpha(\theta) = -\theta_0^{h+1} \frac{\theta}{(\theta^2 + \theta_C^2)^{\frac{h+1}{2}}}. \quad (20)$$

The core radius θ_C can cause complicated behavior of the SPL lens. In this work, we simply choose $\theta_C = 0.05R_0/D_d$ unless we otherwise specify. One can find more detail about the SPL lens in Er & Rogers (2018).

The ratio of geometric to dispersive delay can be also given analytically

$$\eta = \frac{(h-1)\theta_0^{h+1}\theta^2}{(\theta^2 + \theta_C^2)^{\frac{h+3}{2}}}. \quad (21)$$

The maximum ratio will be reached at $\theta = \sqrt{2/(h+1)}\theta_C$,

$$\eta = \frac{(h-1)\theta_0^{h+1}(h+1)^{\frac{h+1}{2}}}{(h+3)^{\frac{h+3}{2}}\theta_C^{h+1}} \propto \frac{\lambda^2 n_0 R_0^h}{\theta_C^{h+1}}. \quad (22)$$

A small core radius θ_C will cause two effects. First, the large geometric delay will only appear at small radius, i.e., describes a small cross section near the lens. On the other hand, when the density gradient becomes large the geometric delay will be large as well.

We present the dependence of θ_0 (Equation (19)) on the frequency and the number density of electrons in Figure 5. It shows a similar pattern to the exponential models. The magnitude of θ_0 also varies according to the lens redshift and power index. We list the value of θ_0 in Table 2 for a set of selected parameters ($n_0 = 1 \text{ cm}^{-3}$, $\nu = 1 \text{ GHz}$, $R_0 = 10^6$ au).

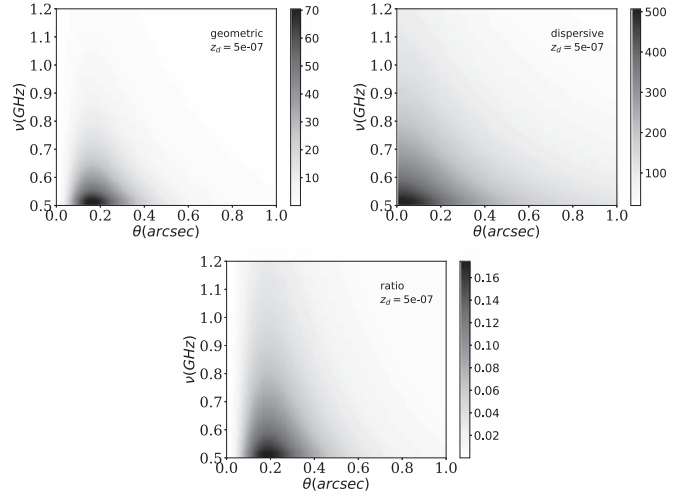


Figure 6. Time delay due to the plasma lensing geometric effect (left), the dispersive effect (right), and their ratio for an SPL model. The lenses are located in Milky Way $z = 5e - 7$ with lens parameters: $h = 2$, $n_0 = 0.1 \text{ cm}^{-3}$, $R_0 = 10^5$ au, and $\theta_C = 0.005R_0/D_d$. In these figures for the lens in the Milky Way, the separation between the lens and source is shown in linear scale for better visibility.

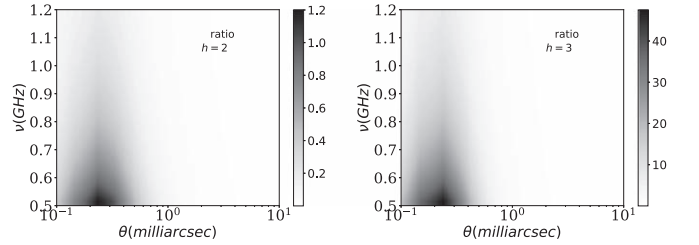


Figure 7. Same as Figure 6, but for lenses at $z = 0.05$ (intervening galaxy). The lens parameters are $n_0 = 0.1 \text{ cm}^{-3}$, $R_0 = 10^6$ au, and the power index is given in each panel.

Table 3

The Dependence of Two Time Delay Terms on the Parameters of the PL Lens Model

Parameter	Geometric Term	Dispersive Term
Lens para.	$\propto n_0^2 R_0^{2h}$	$\propto n_0 R_0^h$
λ	$\propto \lambda^4$	$\propto \lambda^2$

We also compare the time delay between the geometric and dispersive terms for SPL models. In Figure 6, we present a lens in our Galaxy. The projected density at R_0 is 0.05 pc cm^{-3} . While near the central region of the lens (within a hundred au), the density dramatically increases up to a thousand electrons per cm^3 , and DM reaches $\sim 50 \text{ pc cm}^{-3}$. Such a high electron density will not increase the overall average density but can generate a large density gradient and cause strong lensing effects as well as a large geometric time delay. Especially when the plasma lens is in the intervening galaxy (Figure 7), the geometric delay can dominate over the dispersive delay. The lens parameters play a critical role for the geometric delay, but one has to be careful that the relation given in the Table 3 is for PL lens models. A large core radius can totally change the dependence, as it softens the density gradient, and reduces the lensing effect (Er & Rogers 2018).

We compare the two regions on the lens plane: the first where the delay ratio is greater than 0.01, and second where the delay ratio is greater than 0.1. In general these regions depend on the frequency of the observations. What we will present here is the cross section at $\nu = 0.5$ GHz. For the Gaussian lens (Figure 4), the fraction is about 0.56 for $DM_0 = 20 \text{ pc cm}^{-3}$ and 0.7 for $DM_0 = 100 \text{ pc cm}^{-3}$. For the SPL lens in Figure 6, the fraction is about 0.14. If we assume that FRBs are uniformly distributed behind the lens, the fraction can be used to estimate the probability that the geometric effect will contribute a nonnegligible delay. It varies significantly with the lensing properties. For the plasma clump with small scale variations, the contribution from the geometric effect is high.

5. Bias in Estimating the DM

The frequency-dependent time delay can be used to estimate the DM by fitting the frequency-time delay curve of compact radio sources (e.g., Petroff et al. 2016). However, it depends on the assumption that the density gradient can be neglected, i.e., if the density gradient causes deflection of the background radio signal, the frequency-time delay relation will diverge from the general one. Such effects have been noticed in the study of pulsars (e.g., Cordes et al. 2016; Main et al. 2018). As we will see, it is also significant in propagation of FRBs. For the two delay terms in Equation (8), the dispersive term approximately equals the DM. The geometric effect, which is also frequency dependent ($\propto \lambda^4$), will not only cause time delay of the signal, but also change the trajectory of the radio signal. Therefore, the DM that the signal experiences during the propagation will also change according to the frequency. This is also the reason why the dispersive term does not amount to the entire DM. In the end, the estimated DM without plasma lensing is thus biased.

We present an example of plasma lenses in the Milky Way by simulating a toy radio burst signal with an intrinsic Gaussian model of width $\sigma = 5$ milliseconds. We assume that there are no intrinsic delays between frequencies, and propagate it through a clump of plasma. Three different cases of plasma are studied: in the first one, we assume that the plasma is uniformly distributed, i.e., the classical case without lensing. The delay time is calculated from the theoretical prediction

$$t(\nu) = 4.15 \text{ ms} \left(\frac{DM}{\nu^2} \right), \quad (23)$$

where ν is given in units of GHz. In the two other cases we place a plasma lens between us and the source. In the second one, we do not include the geometric delay, and in the third we include all the delay effects from plasma lensing. In the top panel, we adopt a Gaussian lens with $N_0 = 20 \text{ pc cm}^{-3}$, $\sigma = 1000 \text{ au}$. The characteristic radius depends on the frequency. At 1(0.7)GHz, it is about $0''.12(0''.18)$. On the source plane, the corresponding caustic is a circle with radius of about $0''.13(0''.2)$. The radio source is placed at an angular separation of $0''.45$ on the source plane, which is far outside the caustics. At this position the corresponding DM is about 10.7 pc cm^{-3} . In Figure 8, the gray shadows show the three cases from left to right in order: the constant DM, a lens without geometric delay, and the total delay. As a guide for comparison, the blue line represents Equation (23) for a constant DM = 11 pc cm^{-3} . We plot the total delay with

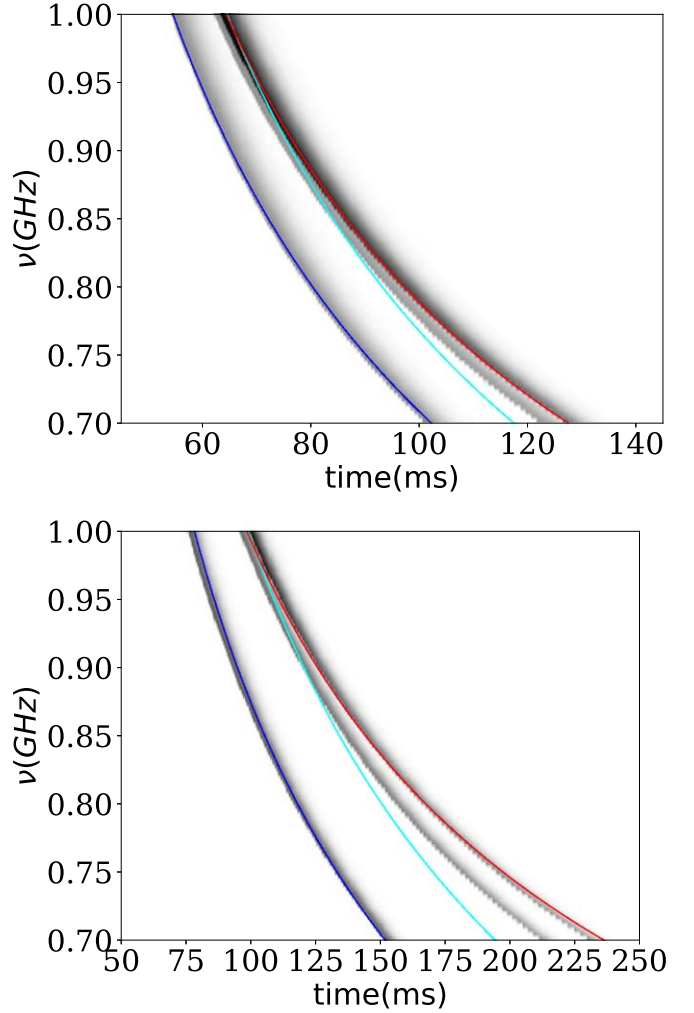


Figure 8. Simulated radio dispersion signal. In both top and bottom panels, from left to right the gray shadow presents the time delay signal on frequency for a constant DM (10.7 pc cm^{-3} in the top panel and 17.3 pc cm^{-3} in the bottom panel), the dispersive delay by the plasma lens, and the total delay by the plasma lens. A Gaussian model ($N_0 = 20 \text{ pc cm}^{-3}$, $\sigma = 1000 \text{ au}$ and located in the Milky Way) is adopted for the lens in the top panel, and a SPL lens ($h = 2$, $n_0 = 0.1 \text{ cm}^{-3}$, $R_0 = 10^5 \text{ au}$) is adopted in the bottom panel. The blue, cyan, and red curve show the analytical curves of Equations (23) and (24). See the text for more details.

another constant DM = 12.2 pc cm^{-3} shown by the cyan line, which nearly overlaps the total simulated gray shadow. As we can see the geometric effect changes the slope of the curve. Such a relationship can be represented by taking into account the higher order effects, as we know that the geometric delay is proportional to λ^4 ,

$$t(\nu) = 4.15 \text{ ms} \left(\frac{DM}{\nu^2} \right) + b \left(\frac{DM^2}{\nu^4} \right), \quad (24)$$

where the same DM is used, and b is a free parameter determined by the geometric effect of the lens. The red line is another fit using Equation (24) with $DM = 11 \text{ pc cm}^{-3}$ and $b = 0.04 \text{ ms}$. Such a fit is different from other empirical relations, for example, Faraday rotation measure caused by the magnetic field (e.g., Cordes & Chatterjee 2019). In the other example (bottom panel of Figure 8), we use an SPL lens with $h = 2$, $n_0 = 0.1 \text{ cm}^{-3}$, $R_0 = 10^5 \text{ au}$ and $\theta_C = 0.005 R_0$, which

gives $\theta_0 \approx 0''.17$, and $0''.21$ of caustics on the source plane at frequency of 1 GHz. At 0.7 GHz, the two scales are $0''.21$ and $0''.29$, respectively. The radio source is separated from the lens by $0''.25$ on the source plane, still out of the caustics. The corresponding $DM = 17.3 \text{ pc cm}^{-3}$. To plot the three analytical curves, we use $DM = 17 \text{ pc cm}^{-3}$ for blue line, $DM = 22 \text{ pc cm}^{-3}$ for the cyan line, and $DM = 17 \text{ pc cm}^{-3}$, $b = 0.07$ for the red line.

6. Discussion

Plasma lensing can cause a significant frequency-dependent time delay effect. The geometric contribution to the time delay may provide a large fraction of the total delay, which strongly depends on the relative distance and properties of the lens.

We found that when the lens is located at the mid-point between the source and observer, refractive lensing can easily cause large time delays, sometimes even larger than the dispersive term. However, such events only happen when the lens perfectly aligns with the source and the density gradient is large. The realistic probability of such a case occurring is low (assuming the cross section is a few milli-arcsec²). On the other hand, when the lens is located within the Milky Way, it also causes a nonnegligible time delay (larger than dispersive delay in all the cases that we presented in this work). We expect the chance of such an event may be higher, and evidence for such refractive effects already exists in some observations of radio sources. Since they have different wavelength dependence, some of the abnormal DMs found in FRBs may be caused by the geometric effects of plasma lensing.

In addition, the frequency-dependent magnification can also provide strong constraints to lensing modeling and help us obtain a better estimate for the electron density as well as the intrinsic properties of the source.

In our study, we adopt the thin lens approximation. As discussed, due to the geometric effect, the radio signal at different frequency experiences different DM, thus the accuracy of the thin lens approximation may not be sufficient when the small scale variation of the plasma is strong, and is worth further study. Such an approximation is widely used in the gravitational lensing community. However, the distribution of ionized gas is more complicated than dark matter halos due to turbulence and related dynamical phenomena. The thin lens approximation with a single lens plane may not be sufficient for such studies. Multi-plane lenses and more complex diffuse distribution models are necessary in future work.

Since FRBs have a large event rate, 10^3 – 10^4 per day all sky (e.g., Cordes & Chatterjee 2019), it is expected that an FRB may pass through a foreground object to reach an observer (Fedorova & Rodin 2019; Prochaska et al. 2019). In this case, the dispersion of the FRBs will deviate from the classic dispersion relation, especially at low frequency. Therefore, a detailed analysis of the FRB dispersion relation would be helpful to study the properties of plasma along the line of sight. Insights into plasma lenses are important because they are difficult to study at all distance scales. Besides lenses in intervening galaxies, even plasma lenses that are near to the observer in the ISM are difficult to detect in general. With knowledge of the detailed dispersion properties of FRBs, one can study the properties of near-source plasma, e.g., the inhomogeneous properties of supernova remnants, pulsar wind nebulae, and H II regions.

We thank the referee for very valuable and detailed constructive comments to the manuscript. We also thank Jenny Wagner, Bing Zhang, Artem Tuntsov, and Guoliang Li for interesting discussions and helpful comments on the draft. X.E. is supported by NSFC grant No. 11873006.

ORCID iDs

Xinzhong Er  <https://orcid.org/0000-0002-8700-3671>
 Yuan-Pei Yang  <https://orcid.org/0000-0001-6374-8313>
 Adam Rogers  <https://orcid.org/0000-0003-2953-2054>

References

- Bannister, K. W., Deller, A. T., Phillips, C., et al. 2019, *Sci*, 365, 565
 Bannister, K. W., Stevens, J., Tuntsov, A. V., et al. 2016, *Sci*, 351, 354
 Bisnovatyi-Kogan, G. S., & Tsupko, O. Y. 2009, *GrCo*, 15, 20
 Bisnovatyi-Kogan, G. S., & Tsupko, O. Y. 2015, *PIPhR*, 41, 562
 Blandford, R., & Narayan, R. 1986, *ApJ*, 310, 568
 Casentini, C., Verrecchia, F., Tavani, M., et al. 2019, arXiv:1911.10189
 Chatterjee, S., Law, C. J., Wharton, R. S., et al. 2017, *Natur*, 541, 58
 CHIME/FRB Collaboration, Amiri, M., Bandura, K., et al. 2019, *Natur*, 566, 235
 Clegg, A. W., Fey, A. L., & Lazio, T. J. W. 1998, *ApJ*, 496, 253
 Cognard, I., Bourgois, G., Lestrade, J.-F., et al. 1993, *Natur*, 366, 320
 Coles, W. A., Kerr, M., Shannon, R. M., et al. 2015, *ApJ*, 808, 113
 Coles, W. A., Rickett, B. J., Gao, J. J., Hobbs, G., & Verbiest, J. P. W. 2010, *ApJ*, 717, 1206
 Cordes, J. M., & Chatterjee, S. 2019, *ARA&A*, 57, 417
 Cordes, J. M., & Lazio, T. J. W. 2002, arXiv:astro-ph/0207156
 Cordes, J. M., Rickett, B. J., Stinebring, D. R., & Coles, W. A. 2006, *ApJ*, 637, 346
 Cordes, J. M., Shannon, R. M., & Stinebring, D. R. 2016, *ApJ*, 817, 16
 Cordes, J. M., Wasserman, I., Hessels, J. W. T., et al. 2017, *ApJ*, 842, 35
 Dai, L., & Lu, W. 2017, *ApJ*, 847, 19
 Deng, W., & Zhang, B. 2014, *ApJL*, 783, L35
 Dong, L., Petropoulos, M., & Giannios, D. 2018, *MNRAS*, 481, 2685
 Donner, J. Y., Verbiest, J. P. W., Tiburzi, C., et al. 2019, *A&A*, 624, A22
 Er, X., & Rogers, A. 2018, *MNRAS*, 475, 867
 Fedorova, V. A., & Rodin, A. E. 2019, *ARep*, 63, 877
 Fiedler, R. L., Dennison, B., Johnston, K. J., & Hewish, A. 1987, *Natur*, 326, 675
 Gwinn, C. R. 2019, *MNRAS*, 486, 2809
 Hessels, J. W. T., Spitler, L. G., Seymour, A. D., et al. 2018, arXiv:1811.10748
 Katz, J. I. 2016, *MPLA*, 31, 1630013
 Keeton, C. R. 2001, arXiv:astro-ph/0102341
 Kerr, M., Coles, W. A., Ward, C. A., et al. 2018, *MNRAS*, 474, 4367
 Lam, M. T., Lazio, T. J. W., Dolch, T., et al. 2019, arXiv:1903.00426
 Lam, M. T., et al. 2018, *ApJ*, 861, 132
 Li, C., & Li, L. 2014, *SCPMA*, 57, 1390
 Li, D., Lin, F. X., Main, R., et al. 2019a, *MNRAS*, 484, 5723
 Li, Z., Gao, H., Wei, J.-J., et al. 2019b, *ApJ*, 876, 146
 Li, Z.-X., Gao, H., Ding, X.-H., Wang, G.-J., & Zhang, B. 2018, *NatCo*, 9, 3833
 Liu, S., Pen, U.-L., Macquart, J.-P., Brisken, W., & Deller, A. 2016, *MNRAS*, 458, 1289
 Lorimer, D. R., Bailes, M., McLaughlin, M. A., Narkevic, D. J., & Crawford, F. 2007, *Sci*, 318, 777
 Main, R., Yang, I. S., Chan, V., et al. 2018, *Natur*, 557, 522
 Marcote, B., Paragi, Z., Hessels, J. W. T., et al. 2017, *ApJL*, 834, L8
 Muñoz, J. B., Kovetz, E. D., Dai, L., & Kamionkowski, M. 2016, *PhRvL*, 117, 091301
 Narayan, R., & Bartelmann, M. 1996, arXiv:astro-ph/9606001
 Pen, U.-L., & King, L. 2012, *MNRAS*, 421, L132
 Pen, U.-L., & Levin, Y. 2014, *MNRAS*, 442, 3338
 Petroff, E., Barr, E. D., Jameson, A., et al. 2016, *PASA*, 33, e045
 Planck Collaboration, Adam, R., Ade, P. A. R., et al. 2016, *A&A*, 594, A1
 Prochaska, J. X., Macquart, J.-P., McQuinn, M., et al. 2019, *Sci*, 366, 231
 Pushkarev, A. B., Kovalev, Y. Y., Lister, M. L., et al. 2013, *A&A*, 555, A80
 Ravi, V., Catha, M., D'Addario, L., et al. 2019, *Natur*, 572, 7769
 Rickett, B. J. 1990, *ARA&A*, 28, 561
 Rogers, A., & Er, X. 2019, *MNRAS*, 485, 5800
 Romani, R. W., Blandford, R. D., & Cordes, J. M. 1987, *Natur*, 328, 324
 Rossi, B., & Twersky, V. 1957, *PhT*, 10, 30

- Schneider, P., Ehlers, J., & Falco, E. E. 1992, *Gravitational Lenses*, Astronomy and Astrophysics Library (Berlin: Springer), 112
- Shannon, R. M., Macquart, J. P., Bannister, K. W., et al. 2018, *Natur*, 562, 386
- Simard, D., & Pen, U.-L. 2018, *MNRAS*, 478, 983
- Simard, D., Pen, U.-L., Ram Marthi, V., & Briskeen, W. 2018, *MNRAS*, 478, 983
- Spitler, L. G., Scholz, P., Hessels, J. W. T., et al. 2016, *Natur*, 531, 202
- Stanimirović, S., & Zweibel, E. G. 2018, *ARA&A*, 56, 489
- Stinebring, D. 2007, in ASP Conf. Ser. 365, SINS—Small Ionized and Neutral Structures in the Diffuse Interstellar Medium, ed. M. Haverkorn & W. M. Goss (San Francisco, CA: ASP), 254
- Stinebring, D. R., McLaughlin, M. A., Cordes, J. M., et al. 2001, *ApJL*, 549, L97
- Tendulkar, S. P., Bassa, C. G., Cordes, J. M., et al. 2017, *ApJL*, 834, L7
- The CHIME/FRB Collaboration, Andersen, B. C., et al. 2019, *ApJL*, 885, L24
- Thornton, D., Stappers, B., Bailes, M., et al. 2013, *Sci*, 341, 53
- Tuntsov, A. V., Walker, M. A., Koopmans, L. V. E., et al. 2016, *ApJ*, 817, 176
- Vedantham, H. K., Readhead, A. C. S., Hovatta, T., et al. 2017, *ApJ*, 845, 90
- Wang, Y. K., & Wang, F. Y. 2018, *A&A*, 614, A50
- Yang, Y.-P., Luo, R., Li, Z., & Zhang, B. 2017, *ApJL*, 839, L25
- Yang, Y.-P., & Zhang, B. 2016, *ApJL*, 830, L31
- Yang, Y.-P., & Zhang, B. 2017, *ApJ*, 847, 22
- Zhang, B. 2018, *ApJL*, 867, L21
- Zheng, Z., Ofek, E. O., Kulkarni, S. R., Neill, J. D., & Juric, M. 2014, *ApJ*, 797, 71